JOURNAL OF PROPULSION AND POWER
Vol. 27, No. 2, March–April 2011

Experimental Study on Combustion Modes in a Supersonic Combustor

Ryou Masumoto*
Tokyo Institute of Technology, Yokohama 226-8502, Japan
Sadatake Tomioka,† Kenji Kudo,‡ Atsuo Murakami,‡ and Kanenori Kato§
Japan Aerospace Exploration Agency, Kakuda 981-1525, Japan
and
Hiroyuki Yamasaki¶
Tokyo Institute of Technology, Yokohama 226-8502, Japan

DOI: 10.2514/1.B34020

Combustion tests were conducted to provide a guideline for designing a supersonic combustor, and an engineering model was established. In the model, particular attention was focused on the length of the constant cross-sectional area combustor and flow conditions. A supersonic combustor with a constant cross-sectional area was employed with several combustor lengths, total temperatures, and equivalence ratios in a directly connected wind tunnel that supplied vitiated airflow with a total pressure of 1.0 MPa, a total temperature of 1500 to 2400 K, and a Mach number of 2.5. No flame holder (e.g., backward-facing step or cavity) and diverging section were attached. Gaseous hydrogen fuel was injected at an angle of 30 deg to the airflow. Four combustion modes were observed: nonignition, weak combustion (with little pressure rise), supersonic combustion, and dual-mode combustion. These combustion modes were organized in terms of combustor length and total temperature at equivalence ratios of 0.2 and 0.4. Although oblique fuel injection was employed to mitigate fuel jet/airflow interaction, the interaction was found to have a sizable effect on the ignition limit. A simple model to predict the minimum combustor length needed to attain supersonic or dual-mode combustion was suggested, and it agreed relatively well with the experimental results. The model was applied to experimental results of a subscale scramjet engine tested under Mach 8 flight conditions at the Japan Aerospace Exploration Agency, Kakuda Space Center, in order to predict the occurrence of combustion (large pressure rise) within a constant area combustor in the engine, and it agreed well with the experimental results.

Nomenclature

A	=	cross-sectional area
C_b	=	mass ratio of burnt fuel
C_d	=	coefficient of discharge
C_f	=	mass ratio of total fuel
c_p	=	specific heat at constant pressure
d_f	=	diameter of fuel injection hole
k	=	experimental constant, degree
L_{comb}	=	combustor length
Ma	=	Mach number
m	=	mass flow rate
N_f	=	number of fuel injection holes
P	=	pressure
q	=	dynamic pressure
R_{univ}	=	universal gas constant
T	=	temperature
T_{atws}	=	airflow temperature at wall surface
V	=	velocity
W	=	molecular weight
X, Y, Z	=	streamwise, lateral, and spanwise locations from duct center at fuel injection location
α	=	fuel injection angle
β	=	shock angle of oblique shock wave
γ	=	specific heat ratio
η	=	mixing, combustion, and kinetic energy efficiency
θ	=	turning angle of oblique shock wave
ρ	=	density
$\tau_i, \tau_{\text{res}}$	=	ignition and residence time
ϕ	=	equivalence ratio

Subscripts

a	=	airflow
b	=	step base
c	=	combustion
f	=	fuel
KE	=	kinetic energy
L	=	local value
m	=	mixing
mix	=	mixture
s	=	behind oblique shock wave
t	=	stagnation condition
w	=	wall
0	=	air heater condition

Presented as Paper 2008-2645 at the 15th AIAA International Space Planes and Hypersonic Systems and Technologies Conference, Dayton, OH, 28 April–1 May 2008; received 20 May 2010; revision received 31 August 2010; accepted for publication 1 September 2010.

*Postgraduate Student, Department of Energy Sciences, 4259 Nagatsuta, Midori-ku. Student Member AIAA.

†Senior Researcher, Kakuda Space Center, Combined Propulsion Research Group, 1 Koganezawa, Kimigaya, Miyagi. Senior Member AIAA.

‡Senior Researcher, Kakuda Space Center, Combined Propulsion Research Group, 1 Koganezawa, Kimigaya, Miyagi.

§Senior Researcher, Kakuda Space Center, Combined Propulsion Research Group, 1 Koganezawa, Kimigaya, Miyagi. Member AIAA.

¶Professor, Department of Energy Sciences, 4259 Nagatsuta, Midori-ku. Member AIAA.

I. Introduction

A ROCKET–RAMJET combined-cycle engine (combination of a scramjet flow pass with embedded rocket engines), which is operated in the ejector-jet mode, ramjet mode, scramjet mode, and rocket mode under a wide range of flight Mach numbers through ascent trajectory, is expected to be the most effective propulsion

system for the space plane [1]. The ramjet and scramjet mode operations are vital parts of the engine operation, as a large part of the acceleration necessary for the space plane is attained under these operations.

As a part of the research efforts on the rocket–ramjet combined-cycle engine, subscale pure scramjet engines were tested at the Ramjet Engine Test Facility (RJTF) [2] under flight conditions of Mach 4, 6, and 8 at the Japan Aerospace Exploration Agency, Kakuda Space Center. The engine had a sidewall compression-type inlet, a few different types of isolators and constant cross-sectional area combustors, a diverging combustor, and an internal nozzle, and some types of struts were installed in the isolator section. Two different combustion modes were observed in the tests [3]. In the case with a small fuel flow rate, the pressure rise due to combustion was so small that the engine hardly generated thrust. On the other hand, combustion was active, and large thrust was produced when the fuel flow rate exceeded a certain threshold. The former and the latter were termed weak combustion and intensive combustion, respectively. As the fuel flow rate was increased, sudden transition of the combustion mode was observed.

In the weak combustion mode, the pressure rise within the combustor was slight, but the level of heat flux was somewhat high in the downstream portion of the combustor, which indicated occurrence of combustion [4,5]. The boundary layer in the combustor remained almost completely attached to the combustor inner wall, and the fuel was scattered within or near the boundary layer. On the other hand, in the intensive combustion mode, the pressure rise within the combustor due to combustion was high and penetrated up to the isolator. The boundary layer in the combustor was largely separated around the fuel injection holes, and almost all of the fuel burned within the shear layer between the separation region and the mainstream [6].

Sunami et al. [7] considered the mechanism of the mode transition from the weak combustion to the intensive combustion as follows. In the weak combustion mode, ignition and combustion of fuel occurred within the boundary layer in the downstream region of the combustor due to high temperature and low velocity. The pressure and temperature increased with the increment of heat release as the fuel flow rate was increased. When the pressure rise exceeded a certain threshold, the reaction region propagated upstream through the boundary layer or through its separation; finally, the intensive combustion mode with separation of the boundary layer around the fuel injector was attained. This mechanism was confirmed by three-dimensional computational simulation [8].

In the series of the engine tests at RJTF, interesting results were obtained. In the tests under Mach 6 flight conditions, shortening the length of the constant cross-sectional area combustor from 160 to 60 mm resulted in the failure of attainment of the intensive combustion, although the length of the diverging combustor (640 mm) was much longer than that of the constant cross-sectional area combustor in both cases [9]. Additionally, Takahashi et al. [10] reported that the transition from self-ignition to flame-holding in a supersonic combustor with a backward-facing step was dominated by the pressure rise near the exit of the constant cross-sectional area combustor. Therefore, the length of the constant cross-sectional area combustor plays an important role in the attainment of the intensive combustion. On the other hand, in the tests under Mach 8 flight conditions at RJTF, an increment of the isolator length by a factor of about three resulted in rather higher pressure within the constant cross-sectional area combustor without fuel injection, so that a much higher pressure rise due to combustion was attained in the case of the longer isolator than in the case of the shorter isolator with little pressure rise, although the configuration of the combustor was the same in both cases [11]. Thus, the flow condition in the constant cross-sectional area combustor is also important for active combustion.

Concerning guidelines for design of the supersonic combustor, what we could find was only Billig's paper [12], in which a minimum combustor inlet pressure was set at one-half atmosphere as a marginal pressure for both ignition and combustion. When designing the subscale scramjet engine tested at RJTF, the combustor geometry was determined using the results of many component studies; the combustor length was $40G$ with a strut and $10G$ without a strut to ensure high combustion efficiency, where G was the throat gap width [13]. However, the engine design based on the combustor length-to-gap-width ratio alone was insufficient, and the failure to attain the intensive combustion was observed as mentioned previously.

The purpose of the present study was to develop a design guideline for the supersonic combustor to attain the intensive combustion. We focused attention on the length of the constant cross-sectional area combustor and the flow conditions, because they played important roles in the attainment of the intensive combustion, as mentioned previously. The constant cross-sectional area combustor is essential to attain the intensive combustion, but it generates no thrust and causes drastic frictional drag. Thus, a model to predict a minimum combustor length to attain the intensive combustion is required. Many studies on models of mixing between fuel and supersonic airflow have been conducted. On the other hand, there have been no studies on the model to determine the combustor configuration (combustor length) and the flow condition that will allow for large thrust. Huber et al. [14] proposed simplified ignition-limit models focused on velocity, temperature, and fuel concentration fields near the fuel injector, and McClinton [15] evaluated the usefulness of the models; with regard to the effect of the combustor length, however, these models are not available. Therefore, a simple model to predict the minimum combustor length was constructed.

In the present study, combustion tests were conducted using a supersonic combustor with a constant cross-sectional area. To pick out the effect of the combustor length on combustion mode, a flame holder was not installed, and oblique fuel injection at an angle of 30 deg was employed. Many studies on supersonic combustors have been conducted with the use of flame holders such as backward-facing steps and cavities, but the amount of heat release (leading to pressure rise) by the flame holder itself is much smaller than that within the combustor, and the contribution of the flame holder to the mode transition from the weak combustion to the intensive combustion is much smaller than that of the combustor length. Oblique fuel injection that would mitigate fuel jet/airflow interaction but sustain smooth mixing of fuel and airflow was used.

In constructing a model to predict the minimum combustor length, there are a large number of parameters to be considered; for example, total pressure (static pressure), total temperature (static temperature), Mach number, isolator length, thickness of boundary layer, diverging angle of combustor, fuel flow rate, etc. As parameters, total temperature and fuel flow rate, as well as combustor length, were chosen and varied, as the former two were also dominant in the attainment of the intensive combustion. Note that, as total temperature was changed with a constant nominal Mach number of 2.5, the main purpose of changing total temperature was to vary static temperature (and velocity) of the airflow entering the supersonic combustor. For reduction of the parameters and simplification of the flowfield, a diverging section was not installed downstream of the constant cross-sectional area combustor.

At the end of the present study, the produced model was applied to the test result at RJTF. The result of a scramjet engine tested under Mach 8 flight conditions was selected. The engine had a sidewall compression-type inlet followed by an isolator, a constant cross-sectional area combustor with fuel injectors, a diverging combustor, and an internal nozzle, and a thick, short strut with a truncated tail was installed in the isolator section and the cross-sectional area combustor section. The engine had a sweptback angle of 45 deg, only in the inlet section. See [11] for more details. Installation of the strut with truncated tail resulted in a rapid expansion of the airflow at the end of the strut and suppressed the upstream penetration of the downstream reaction region into the constant area combustor (around fuel injector), so that the flowfield within the constant area combustor became similar to that within the supersonic combustor tested in the present study. Consequently, the model could predict the occurrence of combustion (large pressure rise) within the constant area combustor in the scramjet engine.

Actually, the intensive combustion includes two combustion modes; that is, supersonic combustion and dual-mode combustion. In the present study, the latter two were used.

II. Experimental Apparatus

A. Wind-Tunnel Facility and Test Apparatus

A supersonic combustor was directly connected to a blowdown-type wind tunnel. A vitiated air heater (a hydrogen and air combustion heater with oxygen replenishment) was used to generate high-enthalpy airflow supplied to the combustor. The mole fraction of oxygen was adjusted to be equal to that of standard air. The total temperature of the test gas $T_{t,0}$ was 1500 ± 50 to 2400 ± 50 K, and the total pressure $P_{t,0}$ was 1.0 ± 0.06 MPa. The test gas was accelerated by a two-dimensional heat-sink nozzle to Mach 2.5. The experimental condition was conformed within an error of $\pm 5\%$.

A schematic diagram of the rectangular supersonic combustor is shown in Fig. 1 with the nozzle and an isolator, as well as the coordinate system used in the present study. The test section consisted of a constant area isolator, a constant area combustor, and an expansion part. The reason for the utilization of the expansion part is described later. The cross-sectional area was changed from 32×147.3 mm in the isolator and the combustor to 62×147.3 mm in the expansion part. The nominal Mach number of the core flow at the isolator inlet was 2.5. The isolator length was 410 mm. Pitot pressure measurements at the combustor inlet showed that Mach number and unit Reynolds number of the core flow at $T_{t,0} = 2000$ K were 2.2 and 7.5×10^6 m^{-1}, respectively, and that Mach number, unit Reynolds number, boundary-layer thickness, and displacement thickness of the boundary layer at $T_{t,0} = 800$ K were 2.2, 2.9×10^7 m^{-1}, 15 mm, and 3.5 mm, respectively. The combustor length L_{comb} was changed from 90 to 720 mm. There were three fuel injection holes (4 mm in diameter and 32 mm interval in spanwise direction) at the streamwise location of $X = 0$ mm on one sidewall. The coefficient of discharge was 0.79. In tests, room-temperature gaseous hydrogen was injected at sonic speed at an angle of 30 deg to the airflow.

The test apparatus was open to the atmosphere, and back pressure could not be controlled. As the static pressure at the combustor exit was lower than the atmospheric pressure, the airflow may have been affected by the atmospheric pressure. When the pressure at the combustor exit was increased, the flow velocity decreased and the temperature increased; thus, ignition of fuel could occur. Hence, the expansion part was used to prevent the ignition of fuel by an expansion fan and to eliminate the effect of atmospheric pressure on the static pressure at the combustor exit. To confirm the formation of the expansion fan with the recirculation region formed in the upstream portion of the expansion part, static pressure in the recirculation region was constantly monitored during the test.

B. Measurement and Data Reduction

Many pressure taps 1.0 mm in diameter were attached to the sidewall. Wall pressure distribution was measured in the streamwise direction in both sidewalls by two mechanical pressure scanners (Scannivalve Company Model J; range: 0–700 kPa; error: $\pm 0.2\%$ full scale); pressure distributions shown in the present study reflect the averaged pressures at each streamwise location. To mitigate the run-to-run deviation of the test conditions, the measured pressure was normalized with the averaged total pressure of the airflow. The repeatability of the nondimensional pressure measurements was within $\pm 3\%$. Furthermore, chromel–alumel thermocouples (0.5 mm in diameter) were inserted into some of the pressure taps (1.0 mm in diameter) with their junction point being flush with the inner wall surface of the combustor, and the airflow temperature at wall surface T_{atws} was constantly monitored. Note that there was a special gap between the inner wall surface of the pressure tap and the junction point of the thermocouple, and that the measured temperature was not the wall temperature but the airflow temperature. T_{atws} was drastically increased or decreased just after fuel injection. In the present study, the variation in T_{atws} (ΔT_{atws}) due to fuel injection was measured to detect variation in airflow temperature due to ignition.

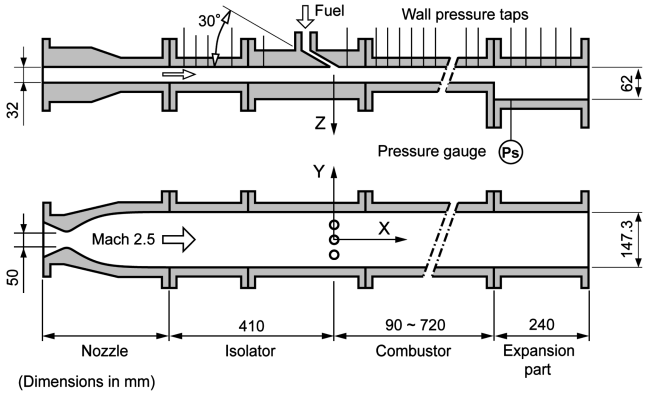

Fig. 1 Schematic diagram of the supersonic combustor.

Pitot pressure measurement and gas sampling were conducted at the combustor exit with a water-cooled sampling rake with 10 probes to investigate the state of burnt gas. The interval of the probe was 10 mm to prevent aerodynamic interaction with the probes. Experiments were repeated to measure local spanwise distributions of gas compositions and pitot pressure, changing the spanwise location of the rake. Reaction quenching during the sampling process was ensured [16]. The sampled gases were analyzed with a gas chromatography for composition of hydrogen, oxygen, and nitrogen with an accuracy of ± 0.3 vol.%. With the composition of the sampled gases and mass flow rates of hydrogen, oxygen, and air fed into the vitiated air heater, the local equivalence ratio (including the reduced reacted fuel) and combustion efficiency (defined as a ratio of reacted fuel to total fuel for an equivalence ratio ≤ 1 or the ratio of reacted oxygen to total oxygen for an equivalence ratio > 1) were calculated. In addition, flow states at the combustor exit were calculated with chemical equilibrium calculation, assuming no heat loss to the combustor wall. The repeatability was within $\pm 9\%$ in the local equivalence ratio, $\pm 11\%$ in local combustion efficiency, and $\pm 4\%$ in local flow states, including the probe-setting error.

III. Results and Discussion

A. Categorization of Combustion Modes

In the present study, four combustion modes were observed: nonignition, weak combustion, supersonic combustion, and dual-mode combustion. Categorization methods of the combustion modes are described in this section.

Figure 2a shows typical wall pressure distributions along the combustor with $T_{t,0} = 2000$ K and $\phi = 0.2$ for various combustor lengths. The horizontal axis represents the streamwise distance from fuel injection hole and the vertical axis represents wall pressure normalized by the averaged total pressure. The pressure distribution without fuel injection is also shown as a reference.

First, with $L_{\text{comb}} = 720$ mm, a large increase in pressure due to combustion was observed not only in the combustor but also in the isolator. The boundary layer in the isolator was separated due to the large pressure gradient and a pseudoshock wave was formed in the isolator. The supersonic airflow was decelerated to subsonic speed through the pseudoshock wave, and the flow was thermally choked at the combustor exit. This much higher pressure mode is generally termed dual-mode combustion. Second, with $L_{\text{comb}} = 420$ mm, the pressure rise due to combustion was confined within the combustor and the pressure gradually increased toward the combustor exit. This combustion phenomenon could be interpreted to mean that the static temperature, the equivalence ratio, and the combustor length were sufficiently large enough to sustain active chemical reaction, but there was an insufficient increase in pressure to separate the boundary layer in the isolator. This case is generally termed supersonic combustion mode. In other conditions, the pressure rises were so small that we could not confirm whether or not the ignition occurred by the pressure distribution alone. Thus, the airflow temperature at wall surface plays an important role.

Figure 2b shows the distribution of the airflow temperature at the wall surface (T_{atws}) under the same conditions as in Fig. 2a, except for the case with $L_{\text{comb}} = 720$ mm. The vertical axis represents the variation in the airflow temperature at the wall surface during 4.4 s after fuel injection. Within the combustor, the increase in T_{atws} was as

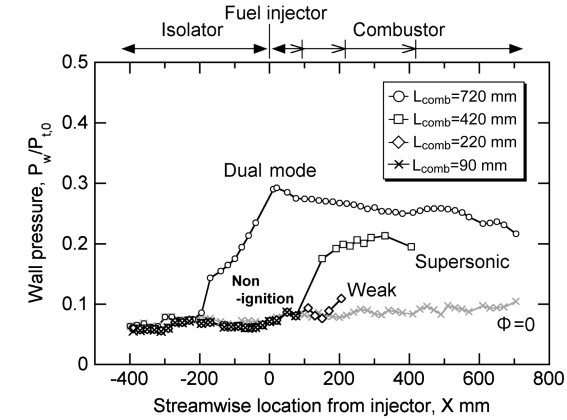

a)

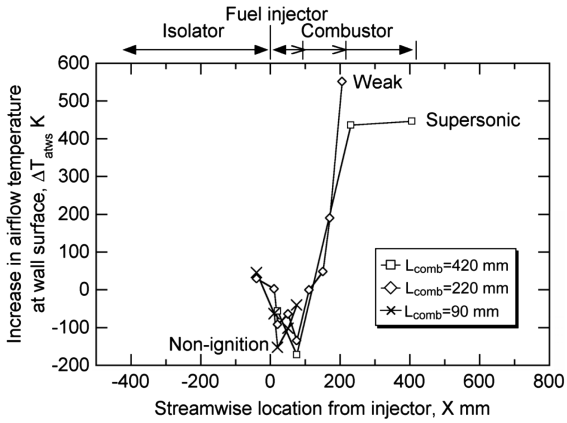

b)

Fig. 2 Typical distributions of a) wall pressure and b) airflow temperature at wall surface ($T_{t,0} = 2000$ K, $\phi = 0.2$).

much as 550 K with $L_{\text{comb}} = 220$ mm, while that with $L_{\text{comb}} = 90$ mm was less than zero. In consequence, we identified that the ignition occurred with $L_{\text{comb}} = 220$ mm and did not occur with $L_{\text{comb}} = 90$ mm. The former, with little increase in pressure but with ignition, was designated as the weak combustion mode, and the latter, without ignition, was designated as nonignition.

B. Features of Each Combustion Mode

Figure 3 shows typical spanwise distributions of local equivalence ratio ϕ_L and local combustion efficiency $\eta_{c,L}$ within the symmetry plane ($Y = 0$) at the combustor exit with $T_{t,0} = 2000$ K and $\phi = 0.2$, with various combustor lengths in nonignition, the weak combustion mode, and the supersonic combustion mode. The vertical axis represents the spanwise distance Z from the center of the combustor, whereas the upper and lower horizontal axes represent $\eta_{c,L}$ and ϕ_L, respectively. In the case of nonignition, $\eta_{c,L}$ was not zero, which indicated that chemical reaction practically occurred. At $Z = -2.5$ mm, $\eta_{c,L}$ showed its maximum value; thus, the reaction was active in the mixing layer between the airflow and the fuel jets. In the case of the weak combustion mode, the penetration height of fuel was high, and $\eta_{c,L}$ showed its maximum value at $Z = 5$ mm, which again indicated active reaction in the mixing layer. In the case of the supersonic combustion mode, fuel was scattered in the whole region of the combustor, and $\eta_{c,L}$ was higher than 0.8, which was the same as in the case of dual-mode combustion, although not shown.

In the case of nonignition, the combustion mode was judged as nonignition by the decrease in the airflow temperature at the wall surface, although the local combustion efficiency was not zero, as shown in Fig. 3. These contradictory results were considered as follows. Figure 4 shows distributions of local total temperature $T_{t,L}$ under the same conditions as in Fig. 3. Note that heat loss to the combustor wall was not taken into account in the calculation; thus, the decrease in total temperature is due to mixing of low-temperature fuel, and the increase is due to heat release by combustion. The local total temperature in the fuel-scattered region decreased only in the case of $L_{\text{comb}} = 90$ mm, although the local combustion efficiency was not zero. Therefore, this case was judged as nonignition.

To evaluate the mixing and combustion performances, cross-section averaged mixing and combustion efficiencies were estimated by assuming that the distributions of local equivalence ratio and local combustion efficiency at arbitrary Y were the same as those in the symmetry plane ($Y = 0$), shown in Fig. 3. The mixing η_m and combustion η_c efficiencies were calculated as

$$\eta_m = \frac{\int_A (\rho V C_f / \phi'_L)\, \mathrm{d}A}{\int_A \rho V C_f \, \mathrm{d}A / \phi'} \tag{1}$$

$$\eta_c = \frac{\int_A \rho V C_b \, dA}{\int_A \rho V C_f \, dA / \phi'} \tag{2}$$

$$\phi'_L = \begin{cases} 1 & (\phi_L \le 1) \\ \phi_L & (\phi_L > 1) \end{cases} \tag{3}$$

$$\phi' = \begin{cases} 1 & (\phi \le 1) \\ \phi & (\phi > 1) \end{cases} \tag{4}$$

where, ρ, V, C_f, C_b, and A were density, velocity, mass ratio of total fuel, mass ratio of burnt fuel, and cross-sectional area, respectively. Results were summarized in Table 1. In the weak combustion mode, mixing efficiency was much higher than combustion efficiency, while both efficiencies were very high in the supersonic combustion mode. This result showed that the mode transition from weak combustion to supersonic combustion was mainly dominated by ignition delay of overall fuel, not by the mixing of fuel and airflow. This mechanism leads to a concept of modeling, discussed later.

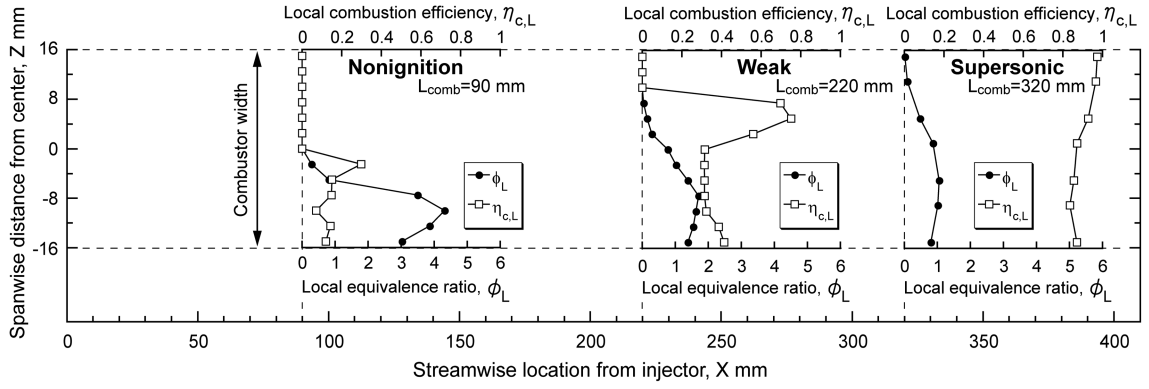

Fig. 3 Spanwise distributions of local equivalence ratio and local combustion efficiency ($T_{t,0} = 2000$ K, $\phi = 0.2$).

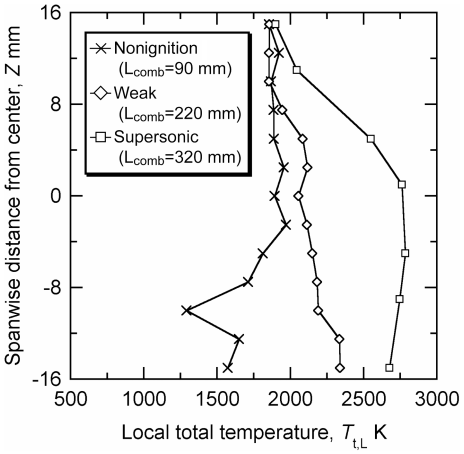

Fig. 4 Spanwise distributions of local total temperature ($T_{t,0}$= 2000 K, $\phi = 0.2$).

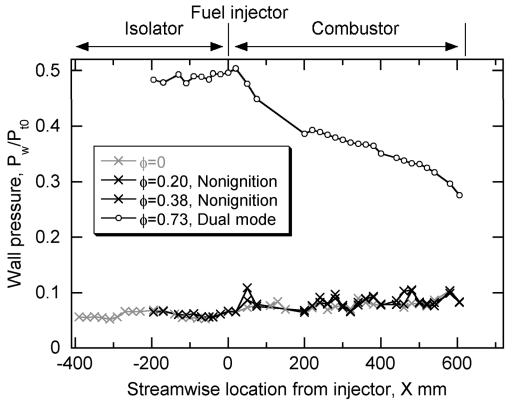

Fig. 5 Wall pressure distributions with $T_{t,0} = 1500$ K and $L_{\text{comb}} = 620$ mm, with several equivalence ratios.

Here, note that the previous assumption led to a larger fuel flow rate than the measured one with a short combustor length, as the local equivalence ratio was much higher than unity. Hence, a fuel flow rate over the cross-sectional area was calculated [integral term of denominator on right-hand side in Eqs. (1) and (2)], and the obtained fuel flow rate was used instead of the measured one in the calculation; the estimated mixing and combustion efficiencies were not actual, but they were valuable as indexes.

C. Effect of Fuel Jet/Airflow Interaction on Combustion Mode

Figure 5 shows wall pressure distributions with $T_{t,0} = 1500$ K and $L_{\text{comb}} = 620$ mm, with several equivalence ratios. The combustion mode was transited from nonignition to dual-mode combustion with increasing equivalence ratio. Simply considering the one-dimensional complete mixing of fuel and airflow, the mixture would become less combustible, because of cold fuel, as the equivalence ratio was increased. However, quite the contrary occurred. The height of the Mach disk formed around the fuel injection hole became higher as the equivalence ratio was increased, which resulted in more intensive fuel jet/airflow interaction and the formation of a stronger bow shock wave and led to the recovery of pressure and temperature of the airflow. Consequently, ignition was more likely to occur with increasing equivalence ratio because of the fuel jet/airflow interaction.

D. Variation of Combustion Modes with Combustor Length

The variations of combustion modes with operating conditions were investigated in terms of the total temperature and the combustor length at two equivalence ratios. Figures 6a and 6b show the results at $\phi = 0.2$ and $\phi = 0.4$, respectively. In the figures, some points show results that the combustion mode changed from the former to the latter during the measurements at 2.4 s, which were critical conditions observed occasionally in the tests.

In both figures, the combustion mode was transited from nonignition to weak, supersonic, or dual-mode combustion as the total temperature and/or the combustor length were increased. In the case of $\phi = 0.2$, the combustion mode was strongly affected by the combustor length, especially at a total temperature of 1500 to 2000 K. In the case of $\phi = 0.4$, once the ignition occurred, almost all of the combustion modes became dual mode due to a larger amount of heat release. Comparing the two cases, there was little difference in the transition condition from nonignition or weak combustion to supersonic combustion or dual-mode combustion (shown by dashed–dotted lines in the figures), as the ignition promotion by the fuel jet/airflow interaction compensated the temperature reduction of the mixture with a larger fuel flow rate.

Table 1 Mixing and combustion efficiencies ($T_{t,0} = 2000$ K, $\phi = 0.2$)

Combustion mode	L_{comb}, mm	η_m	η_c
Nonignition	90	0.37	0.05
Weak	220	0.77	0.28
Supersonic	320	0.99	0.87

IV. Simple Model

In this section, a simple model that predicts the minimum combustor length needed to attain the supersonic or dual-mode combustion is established. In the experiment, local ignition in the mixing layer between the airflow and the fuel jet, or within the boundary layer, did not result in mode transition (a large pressure rise), and the mixing and combustion efficiencies after the transition were rather high (Fig. 3 and Table 1). Thus, the condition in which all of the fuel burned was defined as the threshold of the mode transition. As discussed in Sec. III.B, what dominated the mode transition was not mixing of fuel and airflow but rather ignition delay of the overall fuel. Hence, perfect mixing in an infinitely short distance (the mixing efficiency being unity at the fuel injection location) was assumed. In the modeling, the residence time and the ignition time of the mixture were compared; considering the combustible mixture with a static temperature, a static pressure, and a velocity in flowfield, the mixture ignites when the residence time of the mixture τ_{res} becomes equal to the ignition time (ignition delay time) of the mixture τ_i,

$$\tau_{\text{res}} = \tau_i \tag{5}$$

The flowfield was assumed to be one-dimensional and the gases to be calorically perfect.

A fundamental, simplified model can be made based on one-dimensional mass, momentum, and energy conservation equations about airflow, fuel, and mixture; it was designated as a model without fuel jet/airflow interaction. The meaning of the term of without fuel jet/airflow interaction will be revealed later. Figure 7a shows an illustration of the model without fuel jet/airflow interaction. The symbols 0 and a denote the stagnant state in the vitiated air heater and state of the airflow just upstream of the fuel injector. The airflow at state a and the fuel injected at the sonic speed at state f are completely mixed in an infinitely short distance, and they become the state mix. This mixture flows downstream and ignites at the combustor exit when the residence time of the mixture becomes equal to the ignition time of the mixture; Eq. (5). The relations of each state are as follows:

1) The isentropic relation,

$$\frac{T_{t,a}}{T_a} = 1 + \frac{\gamma_a - 1}{2} Ma_a^2 \tag{6}$$

where $T_{t,a}$, T_a, γ_a, and Ma are total temperature, static temperature, specific heat ratio, and Mach number of the airflow at state a, respectively.

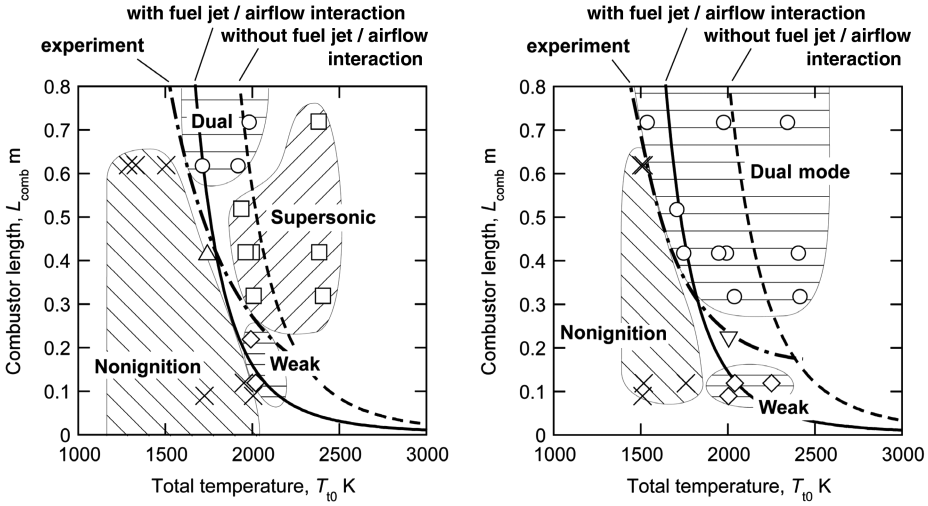

a) $\phi = 0.2$ a) $\phi = 0.4$

Fig. 6 Variation of combustion modes with combustor length and total temperature. (△: nonignition or weak, ▽: weak or dual mode).

2) The mass flow rates of airflow m_a, oxygen in airflow m_{O2}, and fuel m_f are given as

$$m_a = \frac{P_{t,0}A^*}{\sqrt{(R_{\text{univ}}/W_a)T_{t,0}}}\sqrt{\gamma_a\left(\frac{2}{\gamma_a+1}\right)^{(\gamma_a+1)/(\gamma_a-1)}} \tag{7}$$

$$m_{O_2} = 0.2314 m_a \tag{8}$$

$$m_f = 2\phi\frac{W_{H_2}}{W_{O_2}}m_{O_2} \tag{9}$$

where m, A^*, R_{univ}, and W are mass flow rate, cross-sectional area of nozzle throat, universal gas constant, and molecular weight, respectively.

3) For the complete mixing of airflow and fuel, the variables of the state mix were calculated by one-dimensional mass, momentum, and energy conservation equations about the control surface, surrounded by states a, f, and the mix in Fig. 7a. The three conservation equations are

$$m_a + m_f = m_{\text{mix}} \tag{10}$$

$$m_{\text{mix}}V_{\text{mix}} - (m_aV_a + m_fV_f\cos\alpha) = P_aA_a - P_{\text{mix}}A_{\text{mix}} \tag{11}$$

$$m_a(c_{p,a}T_a + \tfrac{1}{2}V_a^2) + m_f(c_{p,f}T_f + \tfrac{1}{2}V_f^2) = m_{\text{mix}}(c_{p,\text{mix}}T_{\text{mix}} + \tfrac{1}{2}V_{\text{mix}}^2) \tag{12}$$

where

$$c_p = \frac{\gamma}{\gamma-1}\frac{R_{\text{univ}}}{W} \tag{13}$$

$$W_{\text{mix}} = \frac{(m_f/W_f)W_f + (m_a/W_a)W_a}{m_f/W_f + m_a/W_a} \tag{14}$$

4) The sonic injection of fuel,

$$V_f = \sqrt{\gamma_f\frac{R_{\text{univ}}}{W_f}T_f} = \sqrt{\frac{2\gamma_f}{\gamma_f+1}\frac{R_{\text{univ}}}{W_f}T_{t,f}}\left(\because\frac{T_{t,f}}{T_f} = \frac{\gamma_f+1}{2}\right) \tag{15}$$

5) For the ignition and residence time, in [14,17], the ignition time was defined as the time it takes for the temperature to increase 5% of the final temperature rise, during which sufficient free radicals or chain carriers are formed to initiate the reaction system, but no appreciable heat is released:

$$\tau_i = \frac{8\times10^{-9}\exp[9600/T_{\text{mix}}]}{P_{\text{mix}}} \tag{16}$$

The residence time of the mixture is defined as

$$\tau_{\text{res}} = \frac{L_{\text{comb}}}{V_{\text{mix}}} \tag{17}$$

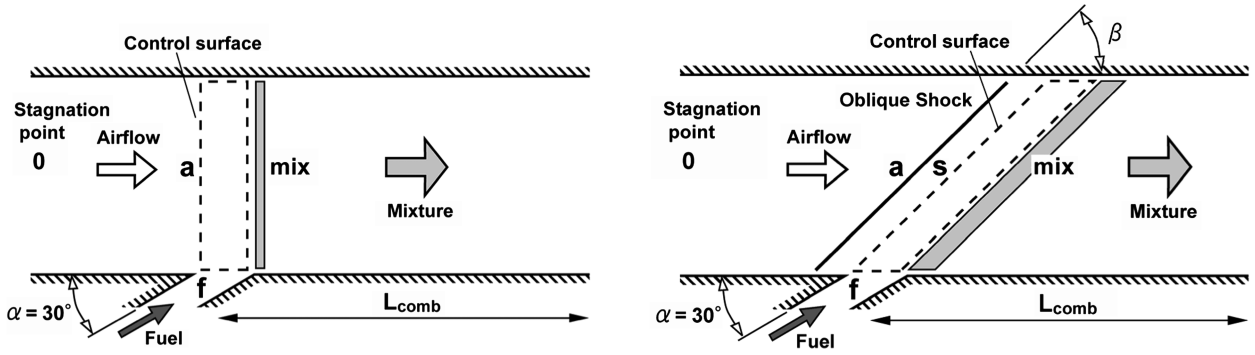

a) Without fuel jet / airflow interaction b) With fuel jet / airflow interaction

Fig. 7 Illustration of a simple model.

6) For the integration of equations, from measurements, we obtained $Ma_a = 2.2$, and $T_{t,a} = 0.95\ T_{t,0}$ due to heat loss. In addition, it was assumed that $\gamma_a = \gamma_f = \gamma_{\text{mix}} = 1.4$, $W_a = 0.029$, and $W_f = 0.002$. Finally, substituting these values and Eqs. (6–17) into Eq. (5), a relation between $T_{t,0}$, L_{comb}, and ϕ is obtained.

In Figs. 6a and 6b, broken lines obtained by the model without fuel jet/airflow interaction and dashed–dotted lines indicating the experimental results are shown. The combustion modes should be supersonic or dual mode in the upper side of the broken lines. However, there were large discrepancies between the model without fuel jet/airflow interaction and the experimental results. In addition, the model without fuel jet/airflow interaction predicted a longer combustor with increasing equivalence ratio, since the static temperature of the mixture became lower due to the cold fuel as the equivalence ratio was increased. Thus, this model could not duplicate the experimental result that ignition was more likely to occur with the increasing equivalence ratio, the reason of which was the fuel jet/airflow interaction (and the recovery of pressure and temperature of the airflow by a bow shock wave). Therefore, the effect of fuel jet/airflow interaction has to be taken into account in the model, so that the increase in the equivalence ratio can promote the ignition. For this purpose, the effect of fuel jet/airflow interaction was modeled by compression of the airflow by an oblique shock wave associated with fuel injection, and the shock angle of the oblique shock wave was given as a function of the equivalence ratio, i.e., fuel injection pressure; this was designated as a model with fuel jet/airflow interaction.

Figure 7b shows an illustration of the model with fuel jet/airflow interaction. The airflow at state a (which is under the same condition of state a in the model without fuel jet/airflow interaction) is compressed by an oblique shock wave into state s, with a shock angle of β and a turning angle of θ. The airflow at state s and the fuel at state f are completely mixed in an infinitely short distance and become state mix. Details are as follows.

1) For the shock and turning angles of the oblique shock wave, the turning angle of the oblique shock wave θ was assumed to be proportional to the height of the Mach disk formed around fuel injector estimated by Cohen et al.'s equation [18]. Thus, the turning angle was given as a function of dynamic pressure,

$$\theta = \frac{k}{1+\cos\alpha}\left(\frac{q_f}{q_a}\right)^{0.5} \tag{18}$$

where k is an experimental constant and α is the fuel injection angle. The dynamic pressure of airflow q_a and the fuel jet q_f are given by Eqs. (19) and (20), respectively:

$$q_a = \rho_a V_a^2/2 = \gamma_a P_a Ma_a^2/2 \tag{19}$$

$$q_f = \rho_f V_f^2/2 = [2(m_f/N_f)(2\gamma_f R_{\text{univ}} T_{t,f} /(\gamma_f+1)W_f)^{1/2}]/(C_d \pi d_f^2) \tag{20}$$

Here, N_f, d_f, and C_d are the number, diameter, and coefficient of discharge of the fuel injection hole, respectively. Substituting Eqs. (7–9), (19), and (20) into Eq. (18), the turning angle is a function of the equivalence ratio.

The shock angle of the oblique shock wave β is obtained as a solution to Eq. (21),

$$\tan\theta = \frac{2\cot\beta(Ma_a^2\sin^2\beta - 1)}{Ma_a^2(\gamma_a + \cos 2\beta) + 2} \tag{21}$$

There are two solutions to Eq. (21): one corresponds to the strong oblique shock wave and the other to the weak one. The strong oblique shock wave resulted in reduction of the airflow speed from supersonic to subsonic, which meant that the supersonic airflow was decelerated to subsonic speed through only one oblique shock wave. This was very unlikely because, actually, within the supersonic combustor, the supersonic airflow was decelerated to subsonic speed through a pseudoshock wave. Therefore, the solution of the weak oblique shock wave (the airflow remained supersonic behind the oblique shock wave) was chosen in the present model. Finally, the shock angle is a function of the equivalence ratio and becomes larger as the equivalence ratio is increased.

2) For the compression by oblique shock wave, the pressure rise ratio by the oblique shock wave was given by the equation of the two-dimensional oblique shock wave:

$$\frac{P_s}{P_a} = \frac{2\gamma_a Ma_a^2\sin^2\beta - (\gamma_a - 1)}{\gamma_a + 1} \tag{22}$$

In the calculation between states a and s, mass and energy conservation were applied, but momentum conservation was violated as the pressure was given in Eq. (22); the error of the momentum conservation was within 7%.

3) For the complete mixing of airflow and fuel, Eqs. (10–12) and (14) are rewritten as (23–26), respectively:

$$m_s + m_f = m_{\text{mix}} \tag{23}$$

$$m_{\text{mix}} V_{\text{mix}} - (m_s V_s + m_f V_f \cos\alpha) = P_s A_s - P_{\text{mix}} A_{\text{mix}} \tag{24}$$

$$m_s(c_{p,s}T_s + \tfrac{1}{2}V_s^2) + m_f(c_{p,f}T_f + \tfrac{1}{2}V_f^2) = m_{\text{mix}}(c_{p,\text{mix}}T_{\text{mix}} + \tfrac{1}{2}V_{\text{mix}}^2) \tag{25}$$

$$W_{\text{mix}} = \frac{(m_f/W_f)W_f + (m_s/W_s)W_s}{m_f/W_f + m_s/W_s} \tag{26}$$

where $m_s = m_a$ and $W_s = W_a$. Note that, in the case of the model without fuel jet/airflow interaction, the variables at state s are identical to those at state a.

4) For the determination of the experimental constant, the value of the experimental constant k in Eq. (18) was specified as follows. Figure 8 shows a typical wall pressure distribution in the case of nonignition. A rather high pressure was observed at $X = 50$ mm (circled in Fig. 8), which would be due to impingement of the bow shock wave formed ahead of the fuel injection hole. Hence, from the wall pressure distribution in the case of nonignition, the pressure rise ratio was calculated based on the difference between the wall pressure with fuel injection and that without fuel injection at $X = 50$ mm. Figure 9 shows the experimentally obtained pressure rise ratio against the dynamic pressure ratio. In the figure, pressure ratios of state s to state a obtained by the model are also shown for several values of k. A value of $k = 6$ was selected as the experimental constant.

A. Comparison with Experimental Results

In Figs. 6a and 6b, solid lines obtained by the model with fuel jet/airflow interaction are shown. The large discrepancies between the

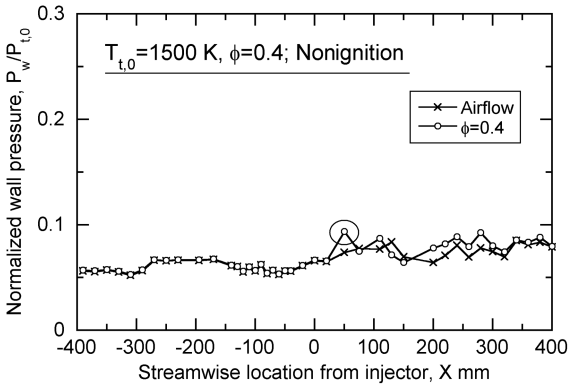

Fig. 8 Typical wall pressure distribution in case of nonignition.

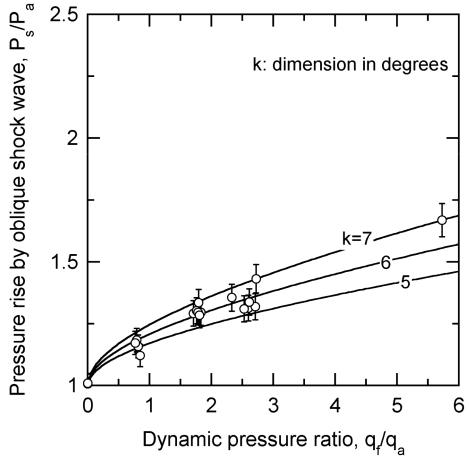

Fig. 9 Relation between pressure rise ratio and dynamic pressure ratio.

model without fuel jet/airflow interaction and experimental results were reduced with the model with fuel jet/airflow interaction by modeling the fuel jet/airflow interaction by the oblique shock wave. Especially in the total temperature range of 1700 to 1800 K, the model with fuel jet/airflow interaction agreed relatively well with the experimental results in spite of such simplification of the modeling. This result indicates that this conceptual model of mode transition phenomena makes sense. In the case of $\phi = 0.4$, the model with fuel jet/airflow interaction overestimated the combustor length in the region with low total temperature because, actually, the increment of the combustor length enhanced the development of the boundary layer, which resulted in the recovery of static temperature and the reduction of velocity and enhanced the ignition. In both cases of $\phi = 0.2$ and 0.4, the model with fuel jet/airflow interaction underestimated the combustor length in the region with high total temperature, because, in practice, there was some distance necessary for mixing of fuel and airflow, although perfect mixing in an infinitely short distance was assumed in the model.

Application of this model to a supersonic combustor with a diverging section as well as a constant cross-sectional area section must result in underestimation of the total combustor length, because the static temperature and pressure within the diverging section decrease and the velocity increases, which suppresses the mode transition. The decreasing/increasing rate depends on the diverging angle. Thus, the diverging angle has to be included in the model; this will be studied in the future.

B. Application of the Model to Test Result at Ramjet Engine Test Facility

The produced model was applied to the test result of a scramjet engine tested at RJTF under Mach 8 flight conditions, as the flowfield within the constant cross-sectional area combustor was similar to that within the supersonic combustor tested in the present study. The reasons of selection of the scramjet engine test were already described in detail at the end of Sec. I. For application of the model to the test result at RJTF, the flow state at the inlet of the constant area combustor (corresponding to the state a in Fig. 7b) had to be obtained in a one-dimensional sense, and a quasi one-dimensional chemical equilibrium calculation [19] was carried out for this purpose. The calculation was based on a mass capture ratio of 0.74 [20].

First, the flow state at the exit of the isolator was calculated based on kinetic energy efficiency η_{KE} with two methods:

1) The value $\eta_{\mathrm{KE}} = 0.98$ was selected so that the resulting pressure level ($0.0023 \times P_{t,0}$) was in good agreement with the measured value ($0.0022 \times P_{t,0}$).

2) An empirical equation about η_{KE} and the Mach number [21] was solved by iterative calculation. In method 1, note that pressure at the midheight line on the sidewall in the scramjet engine was used for the validation of the quasi-one-dimensional calculation. Pressure distribution had a large gradient in the height direction of the engine, and the pressure was low near the top wall and extremely high near the cowl due to the deflection of the airflow and the impingement of shock wave [11]. Although the pressure was low near the top wall, the temperature must have been high and the velocity low, because the engine ingested a thick boundary layer with a height of about 40% of the engine on the top wall, so that the ignition could easily occur near the top wall, even with such a low fuel flow rate that results in ignition failure around the midheight line on the side wall. Thus, the pressure at the midheight line on the sidewall was used as the representative pressure. In method 2, $\eta_{\mathrm{KE}} = 0.996$ and the static pressure of $0.0019 \times P_{t,0}$ were obtained. Utilization of only method 1 was insufficient for our purpose of providing a design guideline for a supersonic combustor, because it meant that we could not estimate the combustor length without actual experiments (without actually measured pressure). Thus, method 2, which needed only a contraction ratio and a mass capture ratio in the inlet, was used; the mass capture ratio could be estimated with an empirical equation (e.g., see [20]).

Second, the flow state at the entrance of the constant cross-sectional area combustor was calculated. Backward-facing steps were installed between the isolator and the combustor, and their projected area was rather large (60% of the projected area of the constant area combustor). Thus, base pressure P_b on the step was estimated by two methods:

1) The airflow was assumed to expand with filling the entire cross section of the constant area combustor.

2) P_b was estimated by an empirical equation [22] as a function of the Mach number. The two methods resulted in deviations of the calculated flow states by about 5%.

Once the flow state at the entrance of the constant area combustor was obtained, the model was directly applied; the overall airflow was compressed by an oblique shock wave and mixed with overall fuel, so that the combustor length to attain a pressure rise due to combustion was estimated as a function of the equivalence ratio. The coefficient of discharge of the fuel injection hole was 0.74.

In Fig. 10, variations of the combustor length with the equivalence ratio estimated by the model are shown for each calculation method of the flow state at the exit of the isolator. The pressure rise due to combustion should be attained in the upper right region of the lines. In the figure, experimental results are also shown. The length of the constant area combustor was 160 mm. As the equivalence ratio was increased from 0.19, the pressure rise due to combustion within the constant area combustor was attained with $\phi = 0.36$ and more. The equivalence ratios estimated by the model agreed well with the experimental ones within the estimated uncertainty.

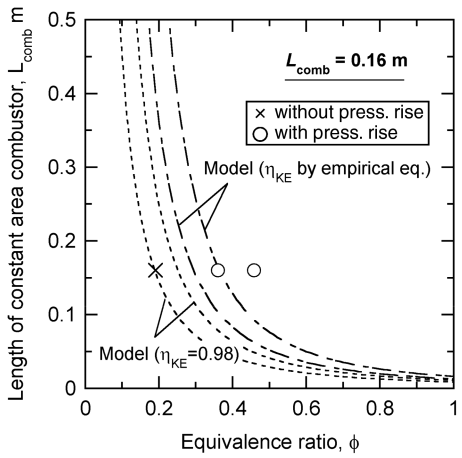

Fig. 10 Variation of combustor length with equivalence ratio in a scramjet engine.

V. Conclusions

To provide a design guideline for a supersonic combustor concerning the combustor length and flow condition, combustion tests of a supersonic combustor were conducted with several combustor lengths, total temperatures, and equivalence ratios in a directly connected wind tunnel that supplied vitiated airflow with a total pressure of 1.0 MPa, a total temperature of 1500 to 2400 K, and a Mach number of 2.5. The supersonic combustor had a constant cross-sectional area and did not have a flame holder (e.g., backward-facing step or cavity) nor a diverging section. In the tests, room-temperature gaseous hydrogen was injected at an angle of 30 deg to the airflow. The following results were obtained:

1) Four combustion modes were observed: nonignition, weak combustion (with little pressure rise), supersonic combustion, and dual-mode combustion.

2) In the weak combustion mode, reaction was active in the mixing layer between the airflow and fuel jet.

3) Although oblique fuel injection was employed, the fuel jet/airflow interaction enhanced the ignition and reaction.

4) The combustion modes were organized in terms of the combustor length and the total temperature at equivalence ratios of 0.2 and 0.4. Comparing the two cases, there was little difference in the transition condition from nonignition or weak combustion to supersonic combustion or dual-mode combustion, as the ignition promotion by the fuel jet/airflow interaction compensated the temperature reduction of the mixture with the larger fuel flow rate.

5) A simple model to predict the minimum combustor length to attain the supersonic or dual-mode combustion was suggested, assuming the compression of airflow by an oblique shock wave and complete mixing of airflow and fuel in an infinitely short distance. In the total temperature range of 1700 to 1800 K, the model agreed relatively well with the experimental results.

6) The model was applied to the experimental results of a subscale scramjet engine tested under Mach 8 flight conditions at RJTF in order to predict the occurrence of the combustion (large pressure rise) within the constant area combustor in the engine. The model agreed well with the experimental results.

Appendix: Flow States at Inlet of Isolator

In the present study, changing the total temperature in a vitiated air heater with a constant Mach number led to variation of the static temperature and velocity of the supersonic airflow. The static temperature and velocity, as well as the Mach number and specific heat ratio at the inlet of isolator (exit of facility nozzle), were calculated with a quasi-one-dimensional chemical equilibrium analysis [23]. Skin friction and heat transfer to the wall were estimated by the van Driest method [24] and the Reynolds analogy.

Variation of the static temperature and velocity with the total temperature and that of Mach number and specific heat ratio are shown in Figs. A1 and A2, respectively. The static temperature and velocity were increased linearly with the total temperature, as the nominal Mach number was constant at 2.5. The Mach number was decreased a little, because a higher total temperature led to a lower Reynolds number and then to a larger skin friction. The specific heat ratio also decreased with the total temperature.

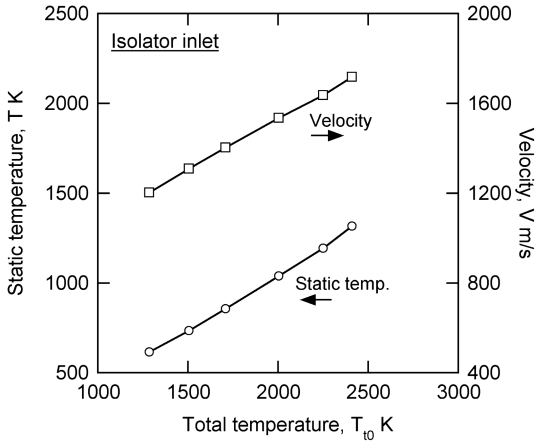

Fig. A1 Variation of static temperature and velocity with total temperature at the inlet of the isolator.

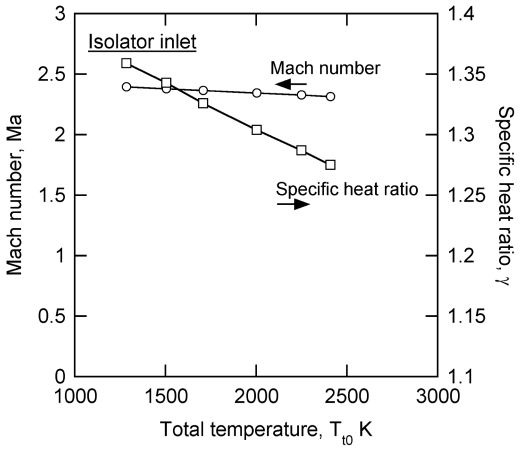

Fig. A2 Variation of Mach number and specific heat ratio with total temperature at the inlet of the isolator.

References

[1] Kanda, T., and Kudo, K., "Conceptual Study of a Combined-Cycle Engine for an Aerospace Plane," *Journal of Propulsion and Power*, Vol. 19, No. 5, 2003, pp. 859–867. doi:10.2514/2.6176

[2] Yatsuyanagi, N., Chinzei, N., Mitani, T., Wakamatsu, Y., Masuya, G., Iwagami, S., Endo, M., and Hanus, G., "Ramjet Engine Test Facility (RJTF) in NAL-KRC, Japan," AIAA Paper 1998-1511, April 1998.

[3] Kodera, M., Tomioka, S., Kanda, T., Mitani, T., and Kobayashi, K., "Mach 6 Test of Scramjet Engine with Boudary-Layer Bleeding and Two-Staged Fuel Injection," AIAA Paper 2003-7049, Dec. 2003.

[4] Kanda, T., Hiraiwa, T., Mitani, T., Tomioka, S., and Chinzei, N., "Mach 6 Testing of a Scramjet Engine Model," *Journal of Propulsion and Power*, Vol. 13, No. 4, 1997, pp. 543–551. doi:10.2514/2.5201

[5] Kanda, T., Sunami, T., Tomioka, S., Tani, K., and Mitani, T., "Mach 8 Testing of a Scramjet Engine Model," *Journal of Propulsion and Power*, Vol. 17, No. 1, 2001, pp. 132–138. doi:10.2514/2.5718

[6] Kodera, M., Sunami, T., and Nakahashi, K., "Numerical Analysis of Combusting Flows in Scramjet," 22nd International Symposium on Space Technology and Science, Japan Society for Aeronautical and Space Sciences and the Organized Committee of the 22nd International Symposium on Space Technology and Science Paper 2000-a-12, Tokyo, May 2000.

[7] Sunami, T., Kodera, M., and Nakahashi, K., "Considerations on Mixing and Combustion of a Scramjet Engine," *Journal of the Japan Society for Aeronautical and Space Sciences*, Vol. 50, No. 576, 2002, pp. 22–29. doi:10.2322/jjsass.50.22 (in Japanese).

[8] Kouchi, T., Mitani, T., Tomioka, S., and Ueda, S., "Transition of Combustion Modes in a Scramjet Engine," 25th International Symposium on Space Technology and Science, Japan Society for Aeronautical and Space Sciences and the Organized Committee of the 25th International Symposium on Space Technology and Science Paper 2006-a-46, Tokyo, June 2006.

[9] Sato, S., Izumikawa, M., Tani, K., Kanda, T., Kudo, K., and Murakami, A., "Mach 6 Combustion Tests of a Scramjet Engine: Effect of Strut and Isolator," *Journal of the Japan Society for Aeronautical and Space Sciences*, Vol. 47, No. 549, 1999, pp. 347–382 (in Japanese).

[10] Takahashi, S., Yamano, G., Wakai, K., Tsue, M., and Kono, M., "Self-Ignition and Transition to Flame-Holding in a Rectangular Scramjet Combustor with a Backward Step," *Proceedings of the Combustion Institute*, Vol. 28, No. 1, 2000, pp. 705–712. doi:10.1016/S0082-0784(00)80272-6

[11] Kobayashi, K., Tomioka, S., Kanda, T., Tani, K., Hiraiwa, T., and Saito, T., "Modified Water-Cooled Scramjet Engine Tested Under M8 Condition," AIAA Paper 2001-3202, July 2001.

[12] Billig, F. S., "Research on Supersonic Combustion," *Journal of Propulsion and Power*, Vol. 9, No. 4, 1993, pp. 499–514. doi:10.2514/3.23652

[13] Masuya, G., and Chinzei, N., "Experiment of Scramjet Combustors and Its Application to a Sub-Scale Engine," 19th International Symposium on Space Technology and Science, Organized Committee of the 19th International Symposium on Space Technology and Science Paper 94-a-07, May 1994.

[14] Huber, P. W., Schexnayder, C. J., Jr., and McClinton, C. R., "Criteria for Self-Ignition of Supersonic Hydrogen-Air Mixtures," NASA TP 1457, 1979.

[15] McClinton, C. R., "Autoignition of Hydrogen Injected Transverse to Supersonic Airstream," AIAA Paper 1979-1239, 1979.

[16] Mitani, T., Takahashi, M., Tomioka, S., Hiraiwa, T., and Tani, K., "Analyses and Application of Gas Sampling to Scramjet Engine Testing," *Journal of Propulsion and Power*, Vol. 15, No. 4, 1999, pp. 572–577. doi:10.2514/2.5465

[17] Pergament, H. S., "A Theoretical Analysis of Non-Equilibrium Hydrogen-Air Reactions in Flow Systems," AIAA 1963-0113, 1963.

[18] Cohen, L. S., Coulter, L. J., and Egan, W. J. Jr., "Penetration and Mixing of Multiple Gas Jets Subjected to a Cross Flow," *AIAA Journal*, Vol. 9, No. 4, 1971, pp. 718–724. doi:10.2514/3.6253

[19] Tomioka, S., Hiraiwa, T., Kobayashi, K., and Izumikawa, M., "Vitiation Effects on Scramjet Engine Performance in Mach 6 Flight Condtion," *Journal of Propulsion and Power*, Vol. 23, No. 4, 2007, pp. 789–796. doi:10.2514/1.28149

[20] Kanda, T., Watanabe, S., Kobayashi, K., Izumikawa, M., and Mitani, T., "Measurement of Mass Capture Ratio of Scramjet Inlets," *Proceedings of the 42nd Conference on Aerospace Propulsion*, Japan Society for Aeronautical and Space Sciences, Tokyo, 2002, pp. 53–58 (in Japanese).

[21] Heiser, W. H., and Pratt, D. T., *Hypersonic Airbreathing Propulsion*, AIAA Education Series, AIAA, Washington, D. C., 1994, pp. 222–226.

[22] Lamb, J. P., and Oberkampf, W. L., "Review and Development of Base Pressure and Base Heating Correlations in Supersonic Flow," *Journal of Spacecraft and Rockets*, Vol. 32, No. 1, 1995, pp. 8–23. doi:10.2514/3.26569

[23] Tomioka, S., Murakami, A., Kudo, K., and Mitani, T., "Combustion Tests of a Stated Supersonic Combustor with a Strut," *Journal of Propulsion and Power*, Vol. 17, No. 2, 2001, pp. 293–300. doi:10.2514/2.5741

[24] van Driest, E, R., "Turbulent Boundary Layer in Compressible Fluids," *Journal of the Aeronautical Sciences*, Vol. 18, No. 3, 1951, pp. 145–160.

C. Segal
Associate Editor